arXiv:1608.05061v1 [cond-mat.quant-gas] 17 Aug 2016

Observation of parity-time symmetry breaking transitions in a dissipative Floquet system of ultracold atoms

Jiaming Li, Andrew K. Harter, Ji Liu, Leonardo de Melo, Yogesh N. Joglekar,* and Le Luo†
Department of Physics, Indiana University Purdue University Indianapolis, Indianapolis, Indiana 46202 USA
(Dated: August 18, 2016)

Open physical systems with balanced loss and gain exhibit a transition, absent in their solitary counterparts, which engenders modes that exponentially decay or grow with time and thus spontaneously breaks the parity-time ($\mathcal{PT}$) symmetry [1–3]. This $\mathcal{PT}$-symmetry breaking is induced by modulating the strength [4] or the temporal profile [5, 6] of the loss and gain, but also occurs in a pure dissipative system without gain [7, 8]. It has been observed that, in classical systems with mechanical [9], electrical [10], and electromagnetic setups [11–14] with static loss and gain, the $\mathcal{PT}$-symmetry breaking transition leads to extraordinary behavior [15–17] and functionalities [18–20]. However, its observation in a quantum system is yet to be realized. Here we report on the first quantum simulation of $\mathcal{PT}$-symmetry breaking transitions using ultracold ^{6}Li atoms. We simulate static and Floquet dissipative Hamiltonians by generating state-dependent atom loss in a noninteracting Fermi gas, and observe the $\mathcal{PT}$-symmetry breaking transitions by tracking the atom number for each state. We find that while the two-state system undergoes a single transition in the static case, its Floquet counterpart, with a periodic loss, undergoes $\mathcal{PT}$-symmetry breaking and restoring transitions at vanishingly small dissipation strength. Our results demonstrate that Floquet dissipation offers a versatile tool for navigating phases where the $\mathcal{PT}$-symmetry is either broken or conserved. The dissipative ultracold Fermi gas provides a starting point for exploring the interplay among dissipation, decoherence, and interactions in open quantum systems.

A fundamental postulate of the quantum theory is that the Hamiltonian of a closed quantum system is Hermitian. It ensures a real energy spectrum and guarantees unitary time evolution. Two possibilities emerge when the quantum system is coupled to a dissipative environment. First, the coupling, such as that to a heat bath, leads to a loss of coherence in the system but preserves the trace of the density matrix, and it can be described by the Lindblad formalism [21]. In the second scenario, the coupling leads to local losses in the system and is reflected in the diminishing trace of the density matrix. Such a system is described by an effective, non-Hermitian Hamiltonian that encodes the energy (or mass) losses to the environment [22].

In special cases, the lossy Hamiltonian H' is equivalent to a Hamiltonian H_{PT} that is invariant under combined parity ($\mathcal{P}$) and time-reversal ($\mathcal{T}$) operations [23]. A key property shared by both Hamiltonians is the $\mathcal{PT}$-symmetry breaking transition that occurs at an exceptional point [24, 25] – a point in the parameter space where two resonant modes of the Hamiltonian become degenerate [26, 27]. By increasing the local loss in H', this transition is predicted to reduce the overall dissipation rate. Its counterpart, the $\mathcal{PT}$-symmetric Hamiltonian H_{PT} models an open system with balanced loss and gain and allows the eigenmode spectrum to evolve from purely real to complex conjugate pairs at the transition. What is remarkable is that the $\mathcal{PT}$-symmetry breaking transition is expected to occur in an open, noninteracting, quantum two-state system – the simplest system possible. In contrast, in the closed-case, symmetry breaking transitions occur only in interacting quantum systems with many degrees of freedom.

Ultracold atoms are powerful quantum simulators where impressive advances have been made towards simulating many-body physics by conserving coherence and minimizing losses [28]. Open-system quantum simulation with ultracold atoms now has become an emerging field in which the interplay between dissipative and unitary dynamics exhibits intriguing properties [29]. In this letter, we present the first quantum simulation of $\mathcal{PT}$-symmetry breaking transitions using ultracold ^{6}Li fermionic atoms by engineering static and Floquet dissipative Hamiltonians. We prepare a noninteracting Fermi gas with the two lowest hyperfine states of the ^{6}Li atom $^2S_{1/2}$ state [30], labeled $|\uparrow\rangle$ and $|\downarrow\rangle$. These two states are coupled by a radio-frequency (rf) field with a coupling strength of J, while an optical beam resonant with the $|\downarrow\rangle \rightarrow {}^2P_{3/2}$ (labeled as $|e\rangle$) transition is used to generate the atom loss in $|\downarrow\rangle$ with an amplitude loss rate of $\Gamma(t)$, as shown in Fig. 1a.

The Hamiltonian for this dissipative two-state system is given by ($\hbar = 1$)

$$H'(t) = J\sigma_x - i\Gamma(t)|\downarrow\rangle\langle\downarrow| = -i\Gamma(t)/2 + H_{PT}(t) \quad (1)$$

where the $\mathcal{PT}$-symmetric Hamiltonian is $H_{PT} = J\sigma_x + i\Gamma(t)\sigma_z/2$. We initialize the system with all atoms in $|\uparrow\rangle$ and let the system evolve for a time t by applying the coherent rf field and the dissipative optical field simultaneously. After that, we measure the atom numbers $N'_\uparrow(t)$ and $N'_\downarrow(t)$ using double-shot absorption imaging, which records the atom numbers of two hyperfine states in a single cloud. Since $N'(t) = \sum_{\sigma=\uparrow\downarrow} N'_\sigma(t)$ is not conserved, we adopt the scaled, normalized total atom number $n(t) = N(t)/N(0)$ to characterize the $\mathcal{PT}$-symmetry breaking transitions. Here $N(t) = \sum_{\sigma=\uparrow\downarrow} N_\sigma(t)$ is the

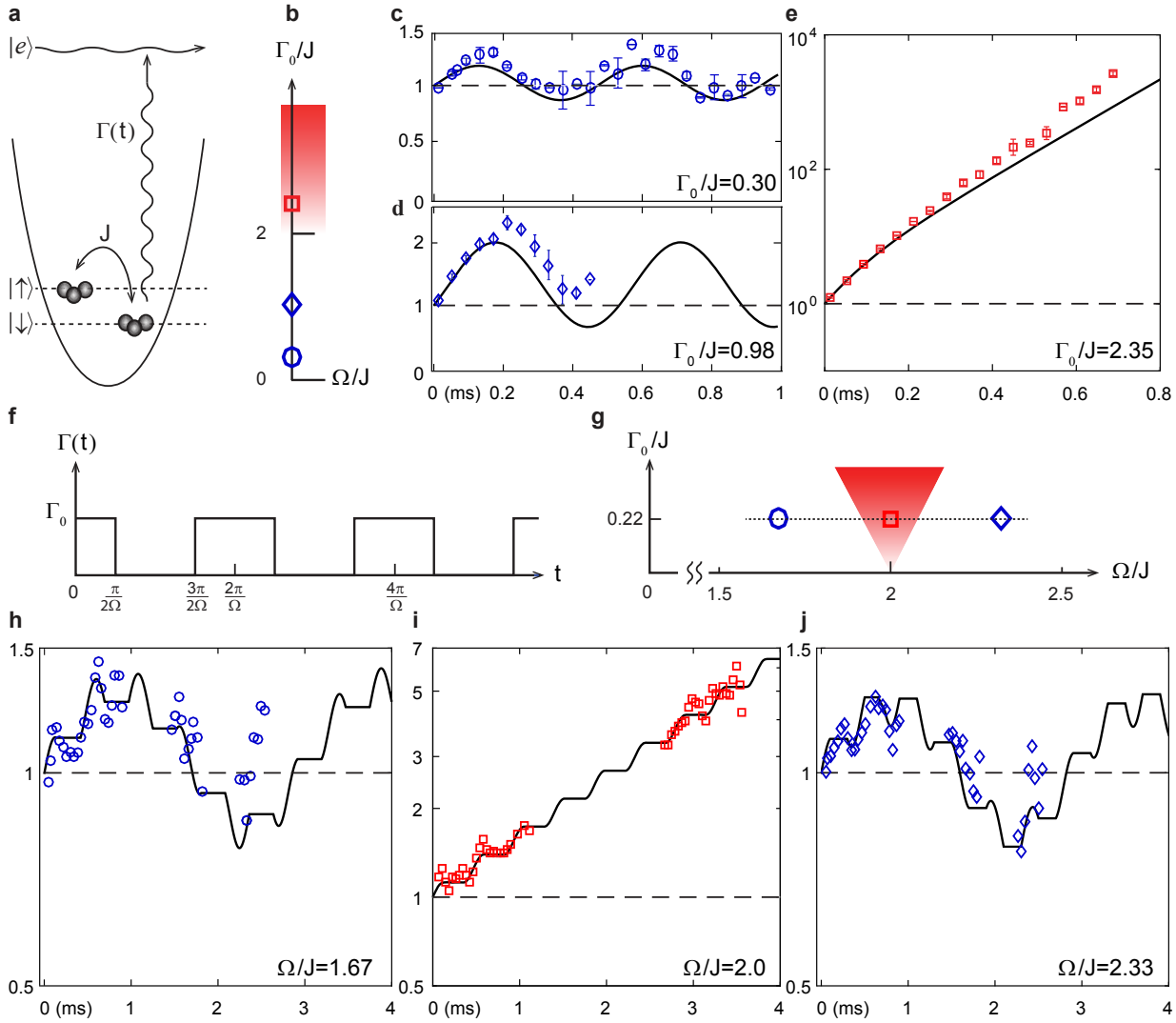

FIG. 1. $\mathcal{PT}$-symmetry breaking transitions in a quantum gas with static and Floquet state-dependent dissipations. **a**, A noninteracting ^{6}Li Fermi gas occupies the lowest two hyperfine states coupled by an rf field $J = \pi\times$ 2.15 kHz. A resonant optical field generates loss $\Gamma(t)$ for $|\downarrow\rangle$ state only. **c-e** and **h-j**, $n(t)$ as a function of time. Symbols are experimental data, solid lines are theory with no free parameter, and dashed lines are the result for a Hermitian system. **b**, For static dissipation, the $\mathcal{PT}$-transition, driven by increasing Γ_0, occurs at $\Gamma_0 = 2J$. **c**, $\Gamma_0 = 0.30J$ and **d**, $\Gamma_0 = 0.98J$ show the $\mathcal{PT}$-symmetric phase, where $n(t)$ oscillates with increasing amplitude and period. **e**, In contrast, $n(t)$ increases exponentially in the $\mathcal{PT}$-broken phase with $\Gamma_0 = 2.35J$. **f**, Square-wave $\Gamma(t)$ is applied to generate the Floquet dissipation by amplitude-modulation of the resonant optical field. **g**, Phase diagram of the Floquet Hamiltonian near the primary-resonance limit shows a triangular $\mathcal{PT}$-broken region. $n(t)$ shows bounded oscillations at $\Omega = 1.67J$ in **h**, an exponential increase at $\Omega = 2.00J$ in **i**, and oscillations again at $\Omega = 2.33J$ in **j**. **h-j**, $\Gamma_0 = 0.22J$ for each case.

total scaled atom number corresponding to the $\mathcal{PT}$-symmetric Hamiltonian (see Methods).

Fig. 1 shows $\mathcal{PT}$-symmetry breaking transitions with static (b-e) and Floquet (f-j) dissipation. For the static dissipation, the $\mathcal{PT}$-symmetry breaking transition is driven by increasing the loss strength $\Gamma(t) = \Gamma_0$ as indicated in Fig. 1b. When $\Gamma_0 < 2J$, the eigenvalues $\pm\lambda = \pm\sqrt{J^2 - \Gamma_0^2/4}$ of H_{PT} are real, and the system is in the $\mathcal{PT}$-symmetric phase. The resulting non-unitary time evolution leads to bounded oscillations in $n(t)$, whose amplitude and period $2\pi/\lambda$ both increase with Γ_0 as shown in Fig. 1c-d. The oscillatory behavior of $n(t)$ indicates that both eigenmodes of H' have lifetimes equal to $2/\Gamma_0$. At the $\mathcal{PT}$-symmetry breaking point $\Gamma_0 = 2J$, the two eigenvalues and corresponding eigenmodes of H_{PT} become degenerate. When $\Gamma_0 > 2J$, the eigenvalues of H_{PT} become complex conjugates, and $n(t)$ increases exponentially with time as observed in Fig. 1e. This qualitatively different behavior of $n(t)$ is due to the emergence of a long-lived mode for the dissi-

pative Hamiltonian H' at the transition point. The lifetime of this mode is given by $2/(\Gamma_0 - \sqrt{\Gamma_0^2 - 4J^2})$ and it increases with the loss amplitude Γ_0, which is a key characteristic of dissipative system in the $\mathcal{PT}$-symmetry broken phase.

When the dissipation is periodic in time, i.e., $\Gamma(t) = \Gamma(t + 2\pi/\Omega)$, the $\mathcal{PT}$-symmetric and $\mathcal{PT}$-broken phases of the Hamiltonian $H_{PT}(t)$ are determined by the eigenvalues of the time evolution operator $G_{PT}(t = 2\pi/\Omega)$ for one period (see Methods). In our experiment, the Hamiltonian $H'(t)$ is realized by square-wave resonant optical pulses with amplitude Γ_0, modulation depth of 100%, and period $2\pi/\Omega$, as shown in Fig. 1f. We focus on the weak-amplitude region in the proximity of the primary resonance, i.e., $\Omega \approx 2J$ and $\Gamma_0 \ll 2J$. The $\mathcal{PT}$ phase diagram in Fig. 1g shows that as the frequency Ω is increased, the system evolves from a $\mathcal{PT}$-symmetric phase to a $\mathcal{PT}$-broken phase (red region), and then back to the $\mathcal{PT}$-symmetric phase again. As shown in Fig. 1h, when $\Omega = 1.67J$, $n(t)$ undergoes bounded oscillations with flat steps that correspond to a unitary evolution which occurs when $\Gamma(t) = 0$. When $\Omega = 2J$, the system is in the $\mathcal{PT}$-broken phase with an exponentially increasing $n(t)$ as shown in Fig. 1i. As the frequency of loss modulation is further increased to $\Omega = 2.33J$, the system returns to the $\mathcal{PT}$-symmetric phase as indicated in Fig. 1j. In these three cases, the loss strength $\Gamma_0 = 0.22J$, is a factor of nine smaller than the static threshold value. This transition, thus, occurs because the Rabi-oscillation-induced occupation of the $|\downarrow\rangle$ state synchronizes with intervals during which the atom loss in $|\downarrow\rangle$ is zero.

To experimentally determine the boundary separating the $\mathcal{PT}$-symmetric and $\mathcal{PT}$ broken phases, we investigate the dependence of atom numbers in each state $N'_\sigma(t, \Gamma_0, \Omega)$ on time, the loss amplitude, and the modulation frequency. Fig. 2a shows the atom numbers of the two states as a function of time in the $\mathcal{PT}$-symmetric phase where $N'_\sigma(t)$ undergo underdamped oscillations. When the system is in the $\mathcal{PT}$-broken phase, the atom numbers show overdamped decay (Fig. 2b). However, the decaying number of atoms and the diverging period of oscillations at the $\mathcal{PT}$ transition point imply that time-dependent state occupations are not best-suited to determine the $\mathcal{PT}$ phase boundary. Instead, in Fig. 2c, we use the atom numbers measured at a fixed time-point $t_m = \pi/(2J)$ as a function of the loss amplitude Γ_0 to determine the transition point. After decreasing initially, the total atom number $N'(\Gamma_0)$ increases with increasing loss strength, signaling the emergence of a long-lived mode and the attendant $\mathcal{PT}$-symmetry breaking transition. The inset of Fig. 2c shows the transition point $\Gamma_{\rm exp}$ obtained by best-fitting the experimental data with $\Gamma_{\rm exp}$ as the only free parameter. The result, $\Gamma_{\rm exp} = (1.92 \pm 0.09)J$ matches the theoretical expectation $\Gamma_{\rm exp} = 2J$ very well.

Compared to the case of a static dissipation, with its

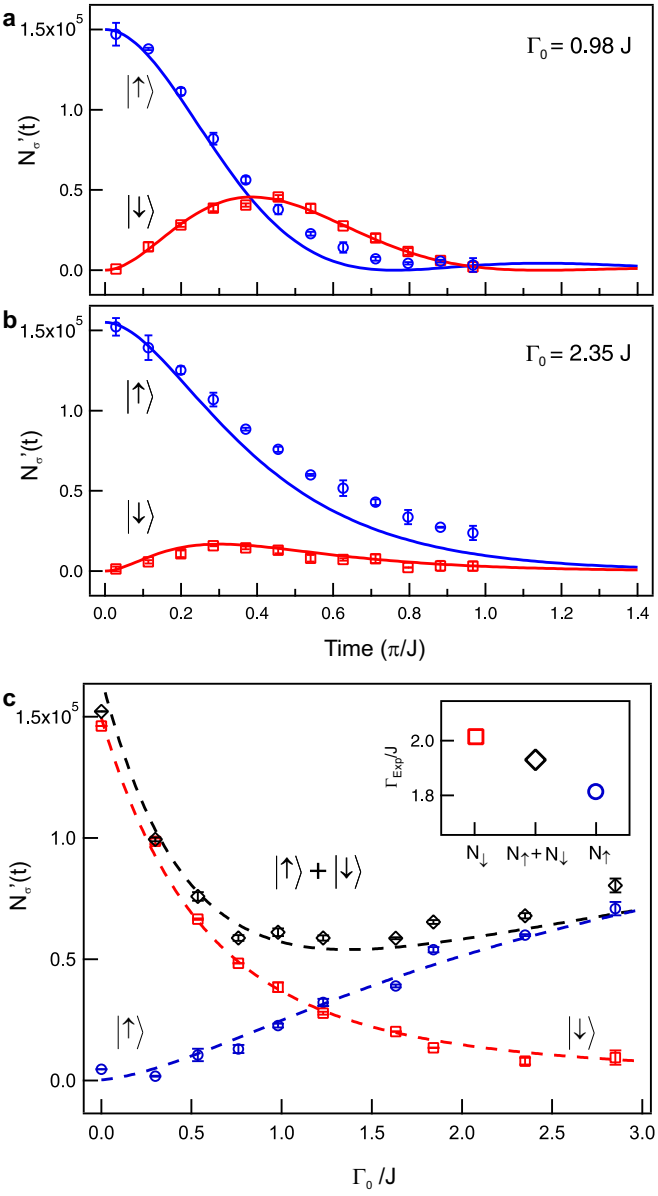

FIG. 2. Determination of the transition point for a static dissipation. Symbols are experimental data, solid lines are theory with no free parameter, dashed lines are best-fit results with the threshold $\Gamma_{\rm exp}$ as the only free parameter. **a**, At $\Gamma_0 = 0.98J$, $N'_\sigma(t)$ undergo underdamped oscillations indicating the $\mathcal{PT}$-symmetric phase. **b**, At $\Gamma_0 = 2.35J$, their overdamped decay is an indicator of a $\mathcal{PT}$-broken phase. **c**, N'_σ measured at $t_m = \pi/(2J)$ as a function of Γ_0 shows a non-monotonic behavior in which $N'(\Gamma_0)$ increases with the loss strength in the broken $\mathcal{PT}$-symmetry region. The inset shows $\Gamma_{\rm exp}$ obtained from the best-fits of the data. In all cases, the initial state of the system is $|\uparrow\rangle$.

two phases separated by a single transition point, the $\mathcal{PT}$-symmetry phase diagram in the case of a Floquet dissipation is rich. The (Γ_0, Ω) parameter-plane has an infinite number of $\mathcal{PT}$-symmetric and $\mathcal{PT}$-broken regions separated by lines of exceptional points [5, 6]. We map

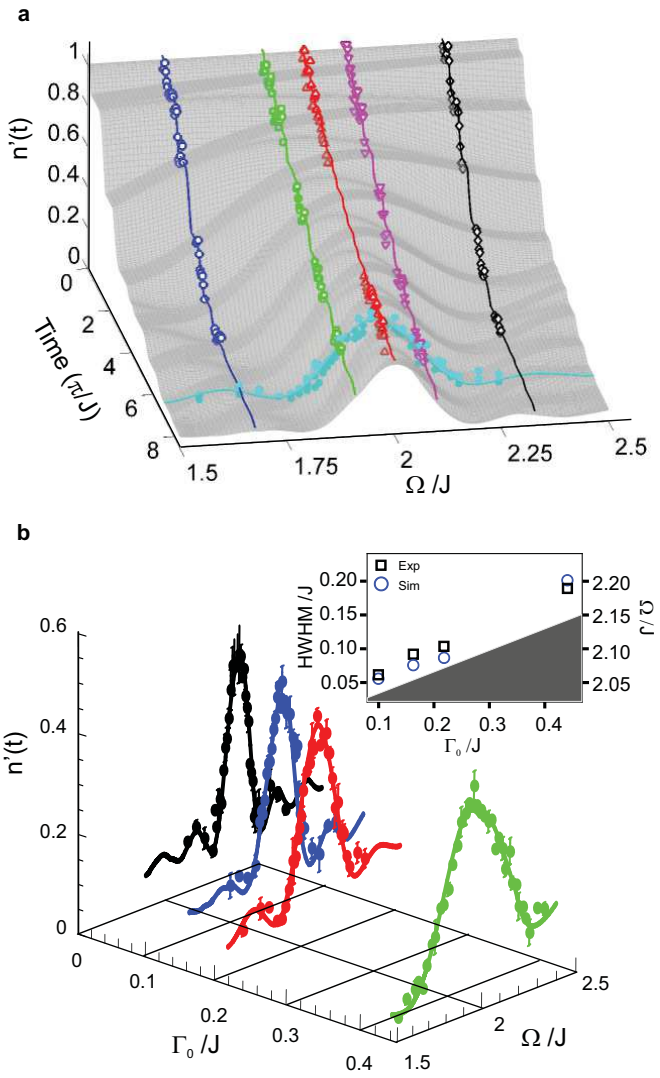

FIG. 3. Determination of the phase diagram of Floquet dissipation near the primary resonance. Symbols are experimental data. Gray surface and solid lines are theory with no free parameters. **a**, $n'(t)$ for $\Omega = 1.67J$ (open blue circles), $\Omega = 1.91J$ (open green squares), $\Omega = 2.00J$ (open red up-triangles), $\Omega = 2.09J$ (open purple down-triangles), and $\Omega = 2.33J$ (open black diamonds), show that $n'(t)$ decays most slowly at the resonance, an indicator of $\mathcal{PT}$-broken phase. A frequency-dependent measurement $n'(\Omega)$ at a fixed time-point $t_m = 7.11(\pi/J)$ (solid cyan dots) also shows a sharp peak at the resonance. For all cases in **a**, $\Gamma_0 = 0.22J$. **b**, $n'(\Gamma_0, \Omega)$ at fixed time-points $t_m(\Gamma_0)$ shows peaks associated with the $\mathcal{PT}$-symmetry broken region: $\Gamma_0 = 0.10J$ and $t_m = 11.37(\pi/J)$ (black), $\Gamma = 0.16J$ and $t_m = 8.53(\pi/J)$ (blue), $\Gamma_0 = 0.22J$ and $t_m = 7.11(\pi/J)$ (red), and $\Gamma_0 = 0.44J$ and $t_m = 4.27(\pi/J)$ (green). The inset shows that the HWHM of the peak increases linearly with the loss amplitude Γ_0, as does the predicted half-width of the $\mathcal{PT}$-symmetry broken (gray) region. The open squares are the Gaussian fits for $n'(\Omega)$ obtained from experimental data, and the open circles are the fits for theoretical simulation.

the phase diagram in the vicinity of the primary resonance $\Omega \approx 2J$ with a square-wave loss-profile. Fig. 3a shows the time evolution of the normalized atom number $n'(t) = N'(t)/N'(0)$ for five modulation frequencies, and the frequency dependence of $n'(\Omega)$ at a fixed time point. For all cases, the loss amplitude $\Gamma_0 = 0.22J$ is an order of magnitude smaller than the static $\mathcal{PT}$-symmetry breaking threshold. We observe that the total atom number loss-rate decreases as $\Omega \to 2J$ and reaches a minimum at the resonance of $\Omega = 2J$. The loss rate increases again when the modulation frequency is increased further. We characterize the two-dimensional phase boundary by experimentally tracking $n'(\Gamma_0, \Omega)$ at a fixed time-point t_m (Fig. 3b). As the loss amplitude increases, the peak of the normalized atom number, which relates to the $\mathcal{PT}$-breaking phase, remains pegged at the resonance and increases in its width. For each Γ_0, we use a Gaussian profile to fit $n'(\Omega)$ and extract the half-width at half-maximum (HWHM) of the peak. The inset in Fig. 3b shows that the extracted HWHM is linearly proportional to the loss strength, as is the predicted half-width of the $\mathcal{PT}$-symmetry broken region (see Methods). It confirms that the fixed-time, frequency-dependent atom number $n'(\Omega)$ is a good indicator to characterize the phase diagram of the Floquet Hamiltonian.

Through the first quantum simulation of parity-time symmetry breaking transitions, we have shown that Floquet dissipation offers a remarkably protean approach for probing non-Hermitian open quantum systems. The results demonstrate that $\mathcal{PT}$-symmetry breaking transitions can be induced by judiciously selected temporal profiles of local dissipation. The ultracold atom system described here provides a platform for systematically investigating the interplay among local dissipation which induces $\mathcal{PT}$-breaking transition, interactions, and decoherence in many-body open quantum systems.

Le Luo is a member of the Indiana University Center for Spacetime Symmetries (IUCSS). This work was supported by IUCRG (JM, LL) and NSF grant no. DMR-1054020 (AH, YJ).

* yojoglek@iupui.edu
† leluo@iupui.edu

[1] C. M. Bender and S. Boettcher, Phys. Rev. Lett. **80**, 5243 (1998).
[2] R. El-Ganainy, K. G. Makris, D. N. Christodoulides, and Z. H. Musslimani, Opt. Lett. **32**, 2632 (2007).
[3] C. M. Bender, Europhys. News **47**, 17 (2016).
[4] K. G. Makris, R. El-Ganainy, D. N. Christodoulides, and Z. H. Musslimani, Phys. Rev. Lett. **100**, 103904 (2008).
[5] Y. N. Joglekar, R. Marathe, P. Durganandini, and R. K. Pathak, Phys. Rev. A **90**, 040101 (2014).
[6] T. E. Lee and Y. N. Joglekar, Phys. Rev. A **92**, 042103 (2015).
[7] T. Eichelkraut, R. Heilmann, S. Weimann, S. Stützer,

F. Dreisow, D. N. Christodoulides, S. Nolte, and A. Szameit, Nat Commun **4**, 1038 (2013).
[8] B. Zhen, C. W. Hsu, Y. Igarashi, L. Lu, I. Kaminer, A. Pick, S.-L. Chua, J. D. Joannopoulos, and M. Soljacic, Nature **525**, 354 (2015).
[9] C. M. Bender, B. K. Berntson, D. Parker, and E. Samuel, American Journal of Physics **81**, 173 (2013).
[10] J. Schindler, A. Li, M. C. Zheng, F. M. Ellis, and T. Kottos, Phys. Rev. A **84**, 040101 (2011).
[11] C. E. Ruter, K. G. Makris, R. El-Ganainy, D. N. Christodoulides, M. Segev, and D. Kip, Nat Phys **6**, 192 (2010).
[12] A. Regensburger, C. Bersch, M.-A. Miri, G. Onishchukov, D. N. Christodoulides, and U. Peschel, Nature **488**, 167 (2012).
[13] S. Bittner, B. Dietz, U. Günther, H. L. Harney, M. Miski-Oglu, A. Richter, and F. Schäfer, Phys. Rev. Lett. **108**, 024101 (2012).
[14] B. Peng, S. K. Ozdemir, F. Lei, F. Monifi, M. Gianfreda, G. L. Long, S. Fan, F. Nori, C. M. Bender, and L. Yang, Nat Phys **10**, 394 (2014).
[15] Z. Lin, H. Ramezani, T. Eichelkraut, T. Kottos, H. Cao, and D. N. Christodoulides, Phys. Rev. Lett. **106**, 213901 (2011).
[16] L. Feng, M. Ayache, J. Huang, Y.-L. Xu, M.-H. Lu, Y.-F. Chen, Y. Fainman, and A. Scherer, Science **333**, 729 (2011).
[17] L. Feng, Y.-L. Xu, W. S. Fegadolli, M.-H. Lu, J. E. B. Oliveira, V. R. Almeida, Y.-F. Chen, and A. Scherer, Nat Mater **12**, 108 (2013).
[18] B. Peng, Ş. K. Özdemir, S. Rotter, H. Yilmaz, M. Liertzer, F. Monifi, C. M. Bender, F. Nori, and L. Yang, Science **346**, 328 (2014).
[19] H. Hodaei, M.-A. Miri, M. Heinrich, D. N. Christodoulides, and M. Khajavikhan, Science **346**, 975 (2014).
[20] L. Feng, Z. J. Wong, R.-M. Ma, Y. Wang, and X. Zhang, Science **346**, 972 (2014).
[21] G. Lindblad, Commun. Math. Phys. **48**, 119 (1976).
[22] N. Moiseyev, Physics Reports **302**, 212 (1998).
[23] A. Guo, G. J. Salamo, D. Duchesne, R. Morandotti, M. Volatier-Ravat, V. Aimez, G. A. Siviloglou, and D. N. Christodoulides, Phys. Rev. Lett. **103**, 093902 (2009).
[24] T. Kato, *Perturbation theory for linear operators* (Springer-Verlag, Berlin, New York, 1966).
[25] W. D. Heiss, Journal of Physics A: Mathematical and General **37**, 2455 (2004).
[26] J. Doppler, A. A. Mailybaev, J. Böhm, U. Kuhl, A. Girschik, F. Libisch, T. J. Milburn, P. Rabl, N. Moiseyev, and S. Rotter, Nature (2016/nature18605).
[27] H. Xu, D. Mason, L. Jiang, and J. G. E. Harris, Nature (2016/nature18604).
[28] I. Bloch, J. Dalibard, and W. Zwerger, Rev. Mod. Phys. **80**, 885 (2008).
[29] M. Müller, S. Diehl, G. Pupillo, and P. Zoller, Advances in Atomic, Molecular, and Optical Physics **61**, 1 (2012).
[30] J. Li, J. Liu, W. Xu, L. deMelo, and L. Luo, Phys. Rev. A **93**, 041401(R) (2016).
[31] G. Zürn, T. Lompe, A. N. Wenz, S. Jochim, P. S. Julienne, and J. M. Hutson, Phys. Rev. Lett. **110**, 135301 (2013).
[32] J. H. Shirley, Phys. Rev. **138**, B979 (1965).

METHODS

Preparing a noninteracting Fermi gas. We prepare ^{6}Li atoms in the two lowest hyperfine states, $|\uparrow\rangle \equiv |F = 1/2, m_F = 1/2\rangle$ and $|\downarrow\rangle \equiv |F = 1/2, m_F = -1/2\rangle$, in a magneto-optical trap. The precooled atoms are transferred into a crossed-beam optical dipole trap (ODT) made by a 100 W IPG Photonics fiber laser. The bias magnetic field is swept to 330 G to implement an evaporative cooling [30]. The trap potential is lowered to 0.04% of the full trap depth in 2.9 s, giving a final trap depth of 2.2 μK for the crossed-beam optical trap. In order to null the interaction between the two hyperfine states, the magnetic field is fast swept to 527.3 G, where the s-wave scattering length of the $|\uparrow\rangle$ and $|\downarrow\rangle$ states is zero [31]. The lifetime of the noninteracting Fermi gas is about 20 seconds, which is three orders of magnitude longer than our typical experimental time. So when the dissipative optical field is absent, this noninteracting Fermi gas can be treated as a closed, two-state quantum system. To prepare a single component Fermi gas in the $|\uparrow\rangle$ state as the initial state, we apply a 5 ms optical pulse with $-2\pi \times 30$ MHz detuning from the $|\downarrow\rangle \rightarrow {}^2P_{3/2}$ transition to blow away atoms in the $|\downarrow\rangle$ state. We typically have about $N = 1.5 \times 10^5$ atoms in a pure $|\uparrow\rangle$ state at temperature $T \approx 0.6$ μK.

A dissipative two-state Rabi system. To generate Rabi oscillations between the two states, we couple them via an rf field with frequency ω and coupling strength J. An optical beam resonant with the $|\downarrow\rangle \rightarrow {}^2P_{3/2}$ transition is used to create the number dissipation (atom loss) in the $|\downarrow\rangle$ state. The resonant-photon recoil energy of 3.5 μK is approximately 50% larger than the trap depth, so atoms absorbing a photon will leave the trap quickly, generating a state-dependent atom loss. The resultant dissipative two-state system is described by a non-Hermitian Hamiltonian ($\hbar = 1$)

$$H = +\frac{\omega_0}{2}\sigma_z - i\frac{\Gamma(t)}{2}(1 - \sigma_z) + 2J\cos(\omega t)\sigma_x, \qquad (2)$$

where $\omega_0 = 2\pi \times 75.6$ MHz is the hyperfine splitting at 527.3 G. When the rf drive is close to resonance, i.e., $\omega \approx \omega_0$, applying the rotating wave approximation for the interacting picture leads to $H' = -i\Gamma(t)/2 + H_{PT}$, where the non-Hermitian, $\mathcal{PT}$-symmetric Hamiltonian is given by

$$H_{PT} = J\sigma_x + i\Gamma(t)\sigma_z/2 = \mathcal{PT}H_{PT}\mathcal{PT}. \qquad (3)$$

Here, $\mathcal{P} = \sigma_x$ and $\mathcal{T} = *$ denotes complex conjugation operation. Starting with an initial state $|\psi(0)\rangle$, the decaying atom numbers for the two states are given by $N'_\sigma(t) \equiv |\langle\sigma|G'(t)|\psi(0)\rangle|^2$ where

$$G'(t) = T\exp\left(-i\int_0^t H'(t')dt'\right), \qquad (4)$$

is the non-unitary time evolution operator obtained via the time-ordered product. It is also useful to define scaled atom numbers $N_\sigma(t) = |\langle\sigma|G_{PT}(t)|\psi(0)\rangle|^2$ where $G_{PT}(t)$ is the corresponding time-evolution operator for $H_{PT}(t)$. It follows that $N_\sigma(t) = N'_\sigma(t) \times \exp(\int_0^t \Gamma(t')dt'/2)$. In a dissipative system, the $\mathcal{PT}$-symmetric phase is signaled by non-decaying, oscillatory $N_\sigma(t)$ and the $\mathcal{PT}$-broken phase is signaled by an exponentially increasing $N_\sigma(t)$.

The rf coupling strength J is measured in the absence of the dissipative optical field, while the atom-number loss rate $2\Gamma_0$ is measured in the absence of the rf coupling. Fig. 4a shows the Rabi oscillation with Rabi frequency $2J$. Fig. 4b shows the atom numbers $N'_\downarrow(t) = N'_\downarrow(0)\exp(-2\Gamma_0 t)$ with a constant dissipative optical field that only couples the $|\downarrow\rangle$ state to the continuum. These measurements are used to calibrate the values of J and Γ_0 for the dissipative two-state Rabi system.

$\mathcal{PT}$ phase diagram: static and dynamic cases. When the resonant optical field is static, i.e., $\Gamma(t) = \Gamma_0$, the eigenvalues of the Hamiltonian H_{PT} are given by $\pm\lambda = \pm\sqrt{J^2 - \Gamma_0^2/4}$ and the $\mathcal{PT}$-symmetry breaking transition occurs at $\Gamma_0 = 2J$. At this exceptional point, H_{PT} is defective [24] and has only one normalized eigenmode $|v\rangle = (1, -i)^T/\sqrt{2}$. Starting with $|\psi(0)\rangle = |\uparrow\rangle$, the atom numbers $N'_\sigma(t)$ are given by

$$N'_\uparrow(t) = e^{-\Gamma_0 t}\left|\cos(\lambda t) + (\Gamma_0/2\lambda)\sin(\lambda t)\right|^2,$$
$$N'_\downarrow(t) = e^{-\Gamma_0 t}\left|i(J/\lambda)\sin(\lambda t)\right|^2, \qquad (5)$$

and the corresponding scaled numbers are $N_\sigma(t) = e^{\Gamma_0 t}N'_\sigma(t)$. Note that for $\Gamma_0 > 2J$, the eigenvalues $\pm\lambda$ become purely imaginary, and the long-time decay rate for $N'(t)$ changes from Γ_0 to $(\Gamma_0 - \sqrt{\Gamma_0^2 - 4J^2})$. When λ is real, the two-state system evolves with period $2\pi/\lambda$ which becomes longer as Γ_0 increases and diverges at the $\mathcal{PT}$-symmetry breaking point. Thus, experimentally probing the dynamics over this time-scale in the vicinity of the transition point is constrained by the residual atoms $N'_\sigma(t \sim 2\pi/\lambda)$ remaining in the trap. Instead, we measured the loss-dependent atom numbers at a fixed time-point, $N'_\sigma(t_m, \Gamma_0)$. We then define a free-parameter dependent eigenvalue $\lambda = \sqrt{\Gamma_{\rm exp}^2 - \Gamma_0^2}/2$, and fit the data in Fig. 2c to Eqs. 5 to extract the experimentally determined $\mathcal{PT}$-symmetry breaking threshold $\Gamma_{\rm exp}$ shown in the inset of Fig. 2c.

For a time-periodic loss $\Gamma(t) = \Gamma(t + 2\pi/\Omega)$, the $\mathcal{PT}$ phase diagram is determined by the eigenvalues of $G_{PT}(t = 2\pi/\Omega)$ or, equivalently, the Floquet Hamiltonian $\mathcal{H}' = i\partial_t - H'$ [32]. For a sinusoidal loss profile, $\Gamma(t) = \Gamma_0\cos(\Omega t)$, the Floquet Hamiltonian $\mathcal{H}$ is tridiagonal in the frequency basis. A perturbative calculation in $\Gamma_0 \ll 2J$ gives $\mathcal{PT}$-symmetry broken phases for frequencies $\Omega \in [\Omega_n - \delta\Omega_n, \Omega_n + \delta\Omega_n]$ where the frequencies $\Omega_n = 2J/(2n+1)$ denote single and multi-photon resonances, and the corresponding half-widths

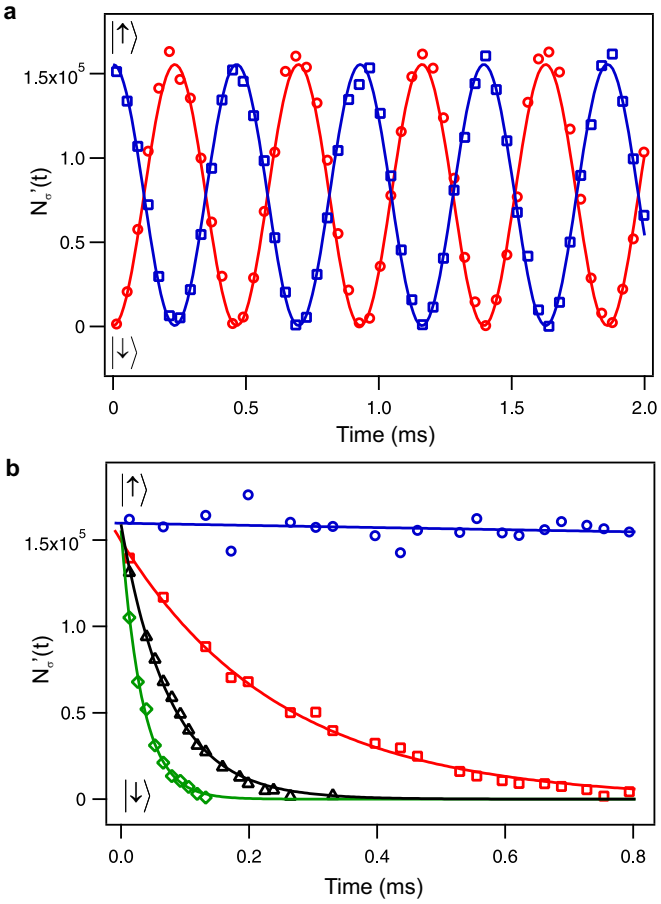

FIG. 4. Characterization of a two-state dissipative Rabi system. Symbols are experimental data. Solid lines are theoretical fits. **a**, In the presence of the rf field but without the dissipative optical field, atom numbers $N'_\sigma(t)$ show Rabi oscillations with a Rabi frequency of $2J = (2\pi) \times 2.15$ kHz. **b**, In the presence of an optical field resonant with $|\downarrow\rangle$ but without the rf field, $N'_\downarrow(t)$ shows an exponential decay: $\Gamma_0 = 0.30J$ (red squares), $\Gamma_0 = 0.98J$ (black triangles), $\Gamma_0 = 2.35J$ (green diamonds). $N'_\uparrow(t)$ remains almost constant during the experimental time. Blue circles show $N'_\uparrow(t)$ when $\Gamma_0 = 0.30J$.

$\delta\Omega_n(\Gamma_0) \propto \Gamma_0(\Gamma_0/J)^n$ devrease in a power-law manner [6]. For experimental simplicity, we consider a square-wave loss profile (Fig. 1(f)),

$$\Gamma(t) = \begin{cases} \Gamma_0 & 0 \le t < \pi/2\Omega, \\ 0 & \pi/2\Omega \le t < 3\pi/2\Omega, \\ \Gamma_0 & 3\pi/2\Omega \le t \le 2\pi/\Omega. \end{cases} \qquad (6)$$

A square-wave loss leads a non-sparse Floquet Hamiltonian $\mathcal{H}'$ and its $\mathcal{PT}$-symmetric counterpart $\mathcal{H}_{PT}$. However, it gives qualitatively the same results as a sine-wave loss-profile, and is much more controllable experimentally. It is also advantageous because $G_{PT}(2\pi/\Omega)$ can be analytically calculated. In the weak-loss limit, the

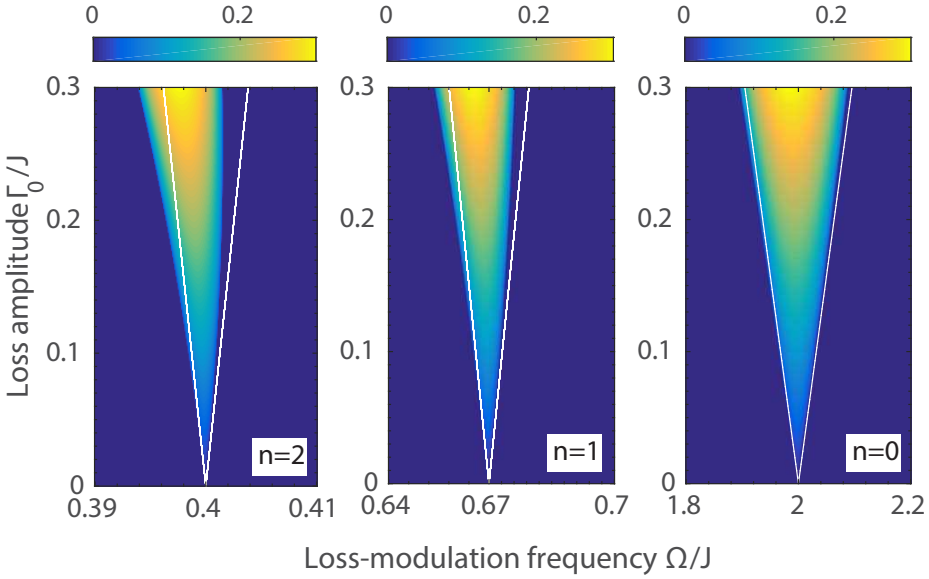

FIG. 5. $\mathcal{PT}$ phase diagram plotting $\Delta\mu(\Omega, \Gamma_0)$ in the vicinity of first three resonances, $\Omega_n = 2J/(2n+1)$ for $n = \{2, 1, 0\}$, shows triangular region of $\mathcal{PT}$-symmetry broken phase ($\Delta\mu > 0$) separated from the $\mathcal{PT}$-symmetric phase ($\Delta\mu = 0$). White lines are the phase boundaries obtained from Eq.(8) and are valid in the limit $\Gamma_0 \ll 2J$.

eigenvalues of $G_{PT}(2\pi/\Omega)$ are given by

$$\mu_\pm(\gamma, \omega) = \cos(2\pi/\omega) \pm i \left[\sin^2(2\pi/\omega) - \gamma^2 \sin^2(\pi/\omega)\right]^{1/2} \tag{7}$$

where $\gamma = \Gamma_0/2J \ll 1$ is the dimensionless loss amplitude and $\omega = \Omega/J$ is the dimensionless frequency. The system is in the $\mathcal{PT}$-broken phase when the two eigenvalues have different magnitudes. It follows from Eq.(7) that it happens when $\Omega \in [\Omega_n - \Delta\Omega_n, \Omega_n + \Delta\Omega_n]$ where

$$\Delta\Omega_n(\Gamma_0) = \frac{\Gamma_0}{\pi}\left(\frac{\Omega_n}{2J}\right)^2. \tag{8}$$

Fig. 5 shows $\Delta\mu = \max|\mu_\pm| - \min|\mu_\pm|$ in the (γ, ω) plane in the vicinity of first three resonances $\Omega_n = \{2J/5, 2J/3, 2J\}$, along with the analytical prediction for the phase boundaries, Eq.(8), shown by white lines. As n increases, Ω_n and the half-width of the broken-$\mathcal{PT}$ symmetry window $\Delta\Omega_n$ both decrease and the linear-phase-boundary approximation is valid at smaller and smaller loss amplitude Γ_0. Due to these constraints, we experimentally investigate the Floquet $\mathcal{PT}$-symmetry breaking transitions in the vicinity of the primary resonance $\Omega_0 = 2J$, where the half-width of the $\mathcal{PT}$-symmetry broken region is given by $\Delta\Omega_0 = \Gamma_0/\pi$.